ORIGINAL PAPER

Asymmetric deformation characteristics and support scheme design of the surrounding rock in deep roadway

Yuxue Chen[1,2] · Liping Li[1,2] · Zongqing Zhou[1,2] · Wenfeng Tu[1,2] · Yuze Zhu[1,2] · Chengshun Shang[1,2]

Abstract
Aiming at the asymmetric deformation of the surrounding rock in the deep roadway, five typical influencing factors of asymmetric deformation have selected: dip angle, buried depth, lithology, lateral pressure coefficient (λ), and height-width ratio (R_{dw}). Taking the surface displacement of the surrounding rock as the measurement index, a method of monitoring and recording the deformation of the full-section node of the roadway has proposed to investigate the surface deformation law of the full-section surrounding rock of the roadway. Based on 25 sets of orthogonal tests, the asymmetric distribution characteristics of surrounding rock deformation under single factor and multiple factors were studied, respectively. The full cross-sectional distribution characteristics of surrounding rock deformation and the main influencing factors of the asymmetric distribution of deformation have got. The most remarkable asymmetric deformation occurs when the dip angle is 45°. λ and R_{dw} significantly influence the asymmetry of the deformation. The coupling relationship between influencing factors has discussed. Based on the level of influencing factors, we briefly gave the prediction of asymmetric deformation of the surrounding rock of the roadway. Closed support measures can significantly reduce the asymmetry of the surrounding rock surface deformation. Combined with the design and optimization of the roadway support scheme, the asymmetric deformation of the surrounding rock has been controlled. This research can provide references for the understanding of the failure characteristics of the surrounding rock in deep inclined formations and the design of deformation control and support schemes.

Keywords Asymmetric deformation · Influencing factor · Deformation stationary point · Deformation prediction

Introduction

Since the 13th Five-Year Plan, the need for deep resource development is increasingly urgent (Xie et al. 2019). Coal will still occupy the dominant position in China's long-term energy mix (Sun et al. 2019). With the extensive development and utilization of shallow coal resources, deep mining has become an inevitable trend, while the surrounding rock of deep roadway is facing with the large deformation, floor heave, and roof collapse problems (He et al. 2018). Especially, when the roadway is constructed in inclined strata, the surrounding rock

✉ Zongqing Zhou
  Zongqing.Zhou@sdu.edu.cn

1 School of Qilu Transportation, Shandong University, Jinan, China

2 Research Center of Geotechnical and Structural Engineering, Shandong University, Jinan, China

deformation is accompanied by remarkable asymmetric deformation phenomenon (He 2011). As known, the burial depth has a remarkable effect on the deformation of surrounding rock (Sun et al. 2019). The dip angle of the strata is a prerequisite for the asymmetry of the surrounding rock deformation in the deep roadway (Sun et al. 2017). As for the deep inclined rock formations, when the roadway is constructed in the hard rock stratum, the lithology of the overburden and underlying has a significant influence on the asymmetry of the surrounding rock deformation, while in the weak rock stratum, the influence is negligible (Chen 2017). However, when the roadway is constructed in the weak rock stratum, the relative deformation of the surrounding rock is significantly larger than that in the shallow mining roadway (Xie et al. 2019). Besides, the asymmetry of surrounding rock deformation is affected by the tunnel shape (Das et al. 2017b; Ding et al. 2019).

For the guarantee of safety production and the increase of economic efficiency, many pieces of research on failure mechanism and deformation control measures for deep roadway have been conducted. The main methods for studying the failure

mechanism in deep roadway include theoretical calculation, model testing (Li et al. 2015), field testing (Jiao et al. 2013; Majcherczyk et al. 2014; Mark et al. 2007), and numerical simulation (Chen et al. 2018a; Das et al. 2017a; Mu et al. 2019). On the mechanism of large deformation failure, researchers have studied the instability and failure patterns, dynamic failure process under kinds of complex engineering-geological conditions (Huang et al. 2013). On the control of surrounding rock deformation, the supporting principle under high-stress condition (Chen et al. 2018b; Shen 2014), combination supporting technology or comprehensive supporting method using bolts, cables, meshes, linings, anchors, shotcrete, and steel arches (Yang et al. 2016), and many reinforcement technologies (Wang et al. 2018) have been studied and applied to control the deformation of the roadway surrounding rock. These studies have controlled the deformation to a great extent in their specified engineering geological environment. However, many studies focused on the shallow tunnels or deep tunnels in the horizontally layered formation, and the large-deformation tunnels control technologies in soft rock (Huang et al. 2018). In particular, when the roadway is constructed in the deep inclined coal measure strata, it will accompany the remarkable asymmetric deformation phenomenon (He et al. 2015; Sun et al. 2017). The asymmetric deformation characteristics and failure mechanism of surrounding rock under the combined action of multiple factors have not particularly conducted. The enhanced support measure in the deep roadway needs further research. Besides, the various stress conditions, geological and geotechnical conditions of the deep mining environments, lead the instability and failure mechanism and supporting measures for deep roadway further complexity. The deformation characteristics and optimal supporting measures of the deep roadway in inclined coal measure strata still need to be further studied.

It is necessary to grasp the asymmetric deformation characteristics of the surrounding rock under single factor and multi-factor coupling and then carry out the design or optimization of the supporting scheme of the surrounding rock under the action of specific influencing factors. In what follows, this paper selected five typical influence factors, dip angle, lateral pressure coefficient, buried depth, lithology, and height-width ratio, to investigate the asymmetry of the surrounding rock deformation. A full-section node displacement monitoring and recording method of the surrounding rock surface has been proposed. Then, the asymmetric deformation characteristics of the surrounding rock under single influencing factor and multi-factor coupling were analyzed, respectively. Discussions have given to provide insights into the interactive relationship of the influencing factors of asymmetric deformation. Finally, the asymmetric deformation characteristics and support scheme design of an on-site roadway were given. We hope that this can provide a reference for the mechanism perceiving and supporting scheme choice of the deep roadway in the inclined strata.

Monitoring method and numerical simulation scheme

The New Austrian tunneling method shows that the surrounding rock itself has a certain self-supporting and maintaining ability after the roadway excavation (Hayati et al. 2014; Ng et al. 2004). After the excavation disturbance, the surrounding rock deformation gradually increases in the disturbed area of the excavated roadway (Yasitli and Erhan 2013). To ensure the stability of the surrounding rock, it is necessary to master the deformation information of the surrounding rock in real time. The displacement monitoring methods, such as the electronic total station (Dong et al. 2014; Dzierzega and Scherrer 2003), sensors, and 3D laser scanning technology, were deployed to monitor the displacement changes of the surrounding rock in model testing (Li et al. 2021) and structural health monitoring (Macpherson et al. 2006; Yang and Oyadiji 2016). However, the deformation monitoring was always limited by the engineering factors and restrained by the number of monitoring points, the data acquisition frequency, and the layout and amount of placed sensors. Besides, the monitoring elements often companied higher requirements for long-term survival. The monitoring data had not yet all-side reflect the deformation of the surrounding rock in real time in the present.

The traditional displacement monitoring method in simulation selects a few typical locations for monitoring. This method is more effective in horizontal rock formations. However, in inclined rock formations, the surrounding rock shows obvious asymmetrical deformation, and the key deformation positions have deviated from the traditional typical monitoring positions, such as archtop, arch shoulder, arch foot, and arch bottom. Based on this, we want to design a nodes' displacement monitoring method suitable for the full-section surrounding rock.

Monitoring method

As an effective numerical simulation research tool, FLAC 3D is widely used in geotechnical engineering (Zhang 2014). We selected the typical section from the 3D geological model built with FLAC 3D and then set the monitoring points of the surface deformation of the surrounding rock. We monitored the displacement of each monitoring point. The monitoring node arrangement of the typical section is shown in Fig. 1. Besides, the roadway is modelled and assembled in the order shown in the quadrants of Fig. 1.

When dividing the node numbers on the surface profile of the roadway into regions, we found that the node numbers can be divided into eight parts. The eight parts uncorrelated with the quadrants grid density, and the node numbers of each part were all arranged in the arithmetic sequence. Taking point A as the starting point, along the counterclockwise direction, the node numbers in the region AOB and region BOC increased
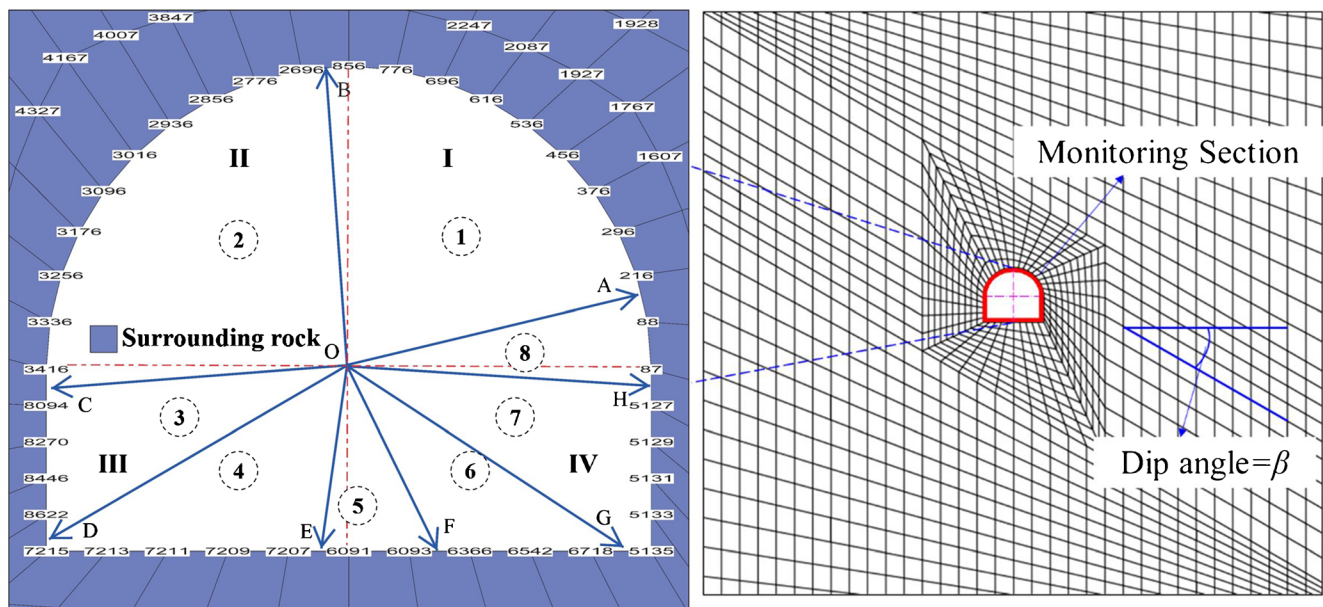
Fig. 1 Monitoring node arrangement of the typical section

by 80 and the region COD and region FOG with the increment 176. The region DOE and region GOH are the node number decreasing area, and the decrement is 2, while the increments of node numbers in the region EOF and region HOA are 2 and 1, respectively. It is noteworthy that the nodes in the region EOF and region HOA are always two nodes. However, the amount of element node and the increment of node number are related to the grid density in the remaining six regions. We have compiled this method into a self-defined program with FISH language in FLAC 3D (Itasca Consulting Group 2012), and the workflow is shown in Fig. 2. Subject to the limitation of the calculation conditions, we had not taken the finer division of the roadway surrounding rock model in this paper. We divided the element nodes according to the distribution rule of the node number shown in Fig. 1. Then we researched the failure characteristics of the asymmetric deformation of the surrounding rock surface in the inclined formations with this node displacement monitoring and recording method.

When arranging the section monitoring points, the lower part arch camber point is set to be the starting number point (monitoring point NO. 1) of the surrounding rock monitoring points and numbered each monitoring point counterclockwise. There are 40 monitoring points on the monitoring section. The two sides of the roadway are often divided into the upper part and lower part according to the dip direction in the inclined strata. Based on the element node distribution in Fig. 2, we regard monitoring point NO. 11 as the roadway arch crown, monitoring point NO. 21 as the upper part arch camber point, monitoring point NO. 26 as the upper part foot, and monitoring point NO. 36 as the lower part foot (Fig. 2).

Numerical simulation scheme setting

Five major contributory factors influencing the asymmetric deformation of roadway surrounding rock are selected. They are dip angle, buried depth, lithology (Lei et al. 2014; Lin et al. 2015), height-width ratio of the roadway (abbreviated as R_{dw} below), and the stratum lateral pressure coefficient (the ratio of horizontal principal stress and vertical principal stress, abbreviated as λ below). In the exploitation of large-scale mineral resources, the common dip angle of the stratum is from 0 to 60°, and the λ is often related to stratigraphic buried depth (Cao et al. 2017). In a complex geological environment, tectonic stress will bring about abnormal regional formation pressure. Studies have shown that structural uplift has little effect on regional abnormal high pressure, which is often accompanied by static pressure or tends to low pressure (Xia et al. 2001). The strong horizontal tectonic compression results in the lateral pressure of the rock formation to be significantly greater than the vertical stress (Zeng et al. 2004), which will make a significant influence on the deformation of the surrounding rock. In situ stress testing, the λ is often adopted to characterize the effect of tectonic stress. In this article, we only consider tectonic compression for the time being and regard the tectonic stress and the λ as the same factors that affect the asymmetric deformation of the surrounding rock. Comprehensive consideration of coal mining technology level and the actuality, the mining depth is reaching 1500m, and the λ commonly changes from 0.5 to 2.0. The deformation of roadway in layered strata is affected by the lithology of overlying and underlying strata. Related research shows that when the roadway is located in the weak rock strata, the change of lithology between the upper and lower rock strata has little impact on the asymmetric
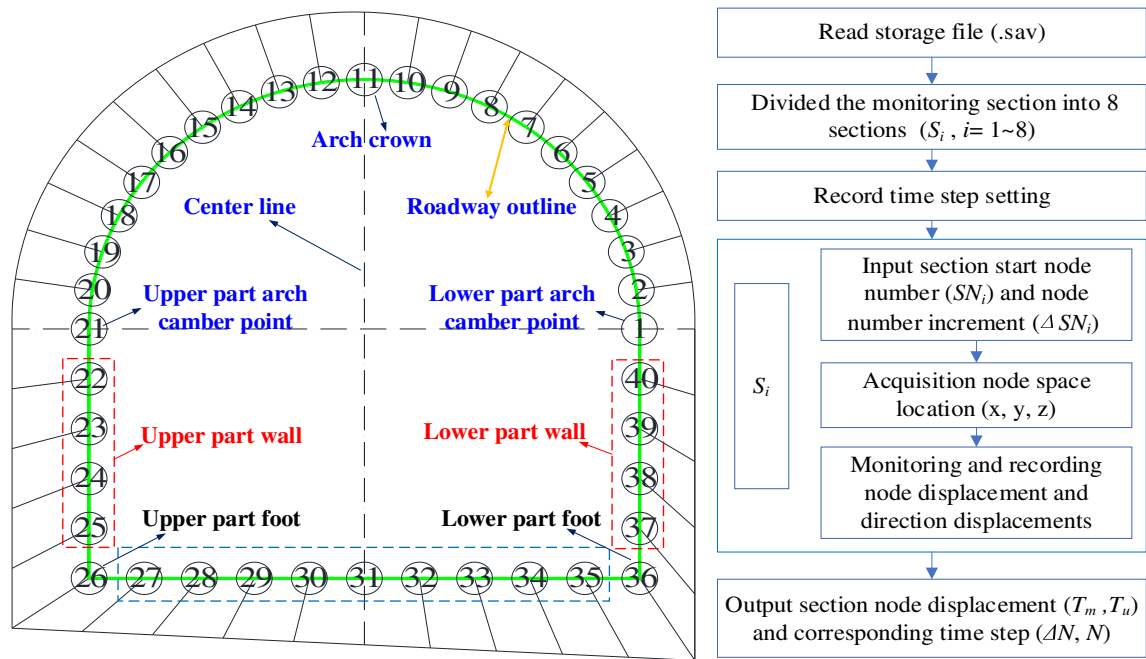
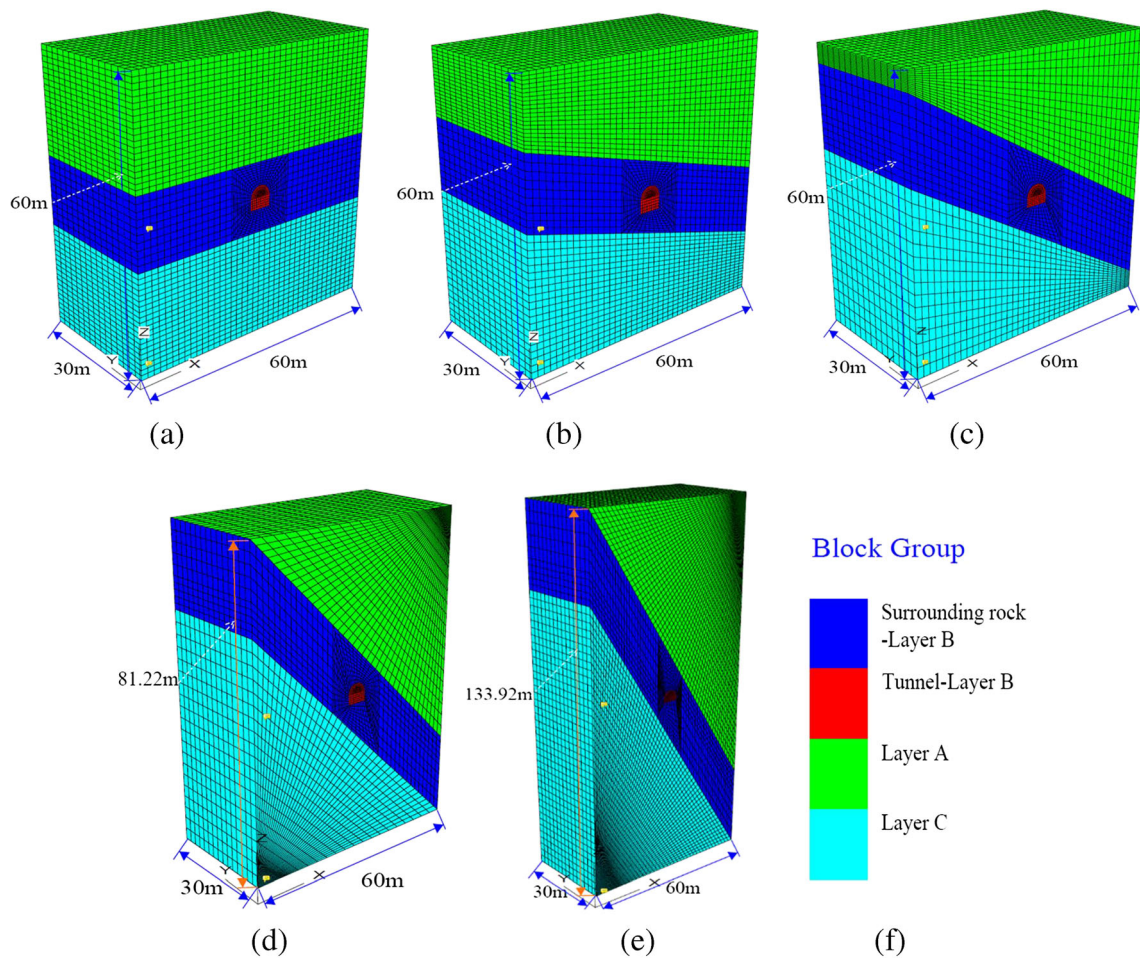Fig. 2 Node number sketch and monitoring and recording work flow

Fig. 3 The models under different dip angles. (**a**) 0°, (**b**) 15°, (**c**) 30°, (**d**) 45°, (**e**) 60°, and (**f**) legend

Table 1   Rock physical parameters

Lithology	Density ρ / (kg/m^3)	Elasticity modulus/ (GPa)	Poisson's ratio/ν	Tensile strength/(MPa)	Cohesion/ (MPa)	Internal friction angle/(°)	Protodyakonov scale of hardness
Mudstone	2533	10.45	0.30	1.58	0.9	30	1~3
Sandy mudstone	2533	16.9	0.23	2.68	1.88	35	3~4
Siltstone	2620	18.01	0.21	4.30	3.1	45	4~7

deformation of surrounding rock (Chen 2017; Chen et al. 2020). So, three common rock strata lithology in mining were selected. The physical parameters of the three lithologies are shown in Table 1. To quantify the softness and hardness of the rock formation, we refer to the Protodyakonov scale of hardness (*f* value) of the selected three rock strata (Table 1). We regard the soft-hard relationship of the rock formation as the lithology level. According to the common roof and floor lithological soft-hard relationship of coal-measure strata, the lithology levels of the layer where the roadway built-in (Layer B), overlying strata (Layer A) and underlying strata (Layer C) were divided into 5 levels, as shown in Table 2.

The variety of roadway usages and mining conditions leads to the variable shape of the roadway section. This paper only studies the straight wall semi-circular arch roadway. We set the different R_{dw} of the roadway under the same width, which is 5 m, and height varies between 3.5 and 5.5 m. We selected five factors affecting the asymmetric deformation of the surrounding rock and set five levels for each factor. The summarized parameters setting of each factor are shown in Table 3. Aimed at the above factors and their levels, we refer to the orthogonal table and select five levels and six factors orthogonal table, namely, $L25$ (5^6), a total of 25 experiment groups (G1~G25). So, the orthogonal table will have a spare column, that is, the last column in Table 4 named null. This does not affect the orthogonal experimental design in the table. Replacing the level values of the corresponding position in the orthogonal table with the actual value of each factor, then got the orthogonal experimental groups' parameters, as shown in Table 4.

The roadway width is 5.0 m; taking the model size effect and boundary effect into consideration, we set the size of the model length and height to be 60 m and the width to be 30 m. Therefore, the model sizes of 0° angel, 15° angle, and 30° angle would have been 60 m long, 30 m width, and 60 m height. For the steeply inclined rock formation, the 45° angle model was 81.22 m height, and the 60° model was 133.92 m height. The numerical models of roadway in each experimental group were established respectively by FLAC 3D, as shown in Fig. 3a~e. The bottom of the model has set to vertical displacement constraint. The around of the model has applied to stress boundary conditions, and the top of the model has set to free boundary, as shown in Fig. 4. After initializing ground stress, the models have solved to the equilibrium state according to the Mohr-Coulomb constitutive model for jointed rock mass damage (Lan et al. 2008). In each model, the deformation and failure over time of surrounding rock of the roadway surface after excavation is recorded according to the monitoring point layout scheme in Fig. 2. As the above 25 models with the same length in Y-axis direction, which is 30m, we set the monitoring section at the middle section Y=15m. The evolving relation of displacement over the solve step of each monitoring point on the roadway surface is extracted from the monitoring data. In the simulation, we found that the maximum displacement (abbreviated as T_m) of some nodes on the roadway section is not the same as the final

Table 2   Lithology and levels setting

NO.	Layer A	Layer B	Layer C	Layers A-B-C soft-hard relationship	Lithology levels
1	Sandy mudstone	Mudstone	Siltstone	Slight hard-soft-hard	I
2	Siltstone	Mudstone	Sandy mudstone	Hard-soft-slight hard	
3	Mudstone	Sandy mudstone	Siltstone	Soft-slight hard-hard	II
4	Siltstone	Sandy mudstone	Mudstone	Hard-slight hard-soft	III
5	Mudstone	Siltstone	Sandy mudstone	Soft-hard-slight hard	IV
6	Sandy mudstone	Siltstone	Mudstone	Slight hard-hard-soft	V

Table 3 Summary of factor levels

Dip angle (β)/°	Lateral pressure coefficient (λ)	Burial depth (H)/m	Lithology	Height-width ratio (R_{dw})
0°	0.5	100	I	0.7
15°	0.67	450	II	0.8
30°	1	800	III	0.9
45°	1.5	1150	IV	1.0
60°	2.0	1500	V	1.1

displacement (abbreviated as T_u). The deformation of some monitoring points will fall to a certain extent during the solution process. In some model tests and simulations, this kind of surrounding rock deformation falls back phenomenon will be observed frequently (Li et al. 2015; Li et al. 2018; Peng et al. 2018), which is mainly caused by the mutual influence of the deformation and migration of the monitoring points on the surface of the roadway. So, we plotted the T_m and T_u curves of the monitoring points on the same coordinate axes.

Result and analysis

Using the nodes' displacement monitoring and recording method designed in Fig. 2, the displacement of the monitoring

Table 4 Test parameters design

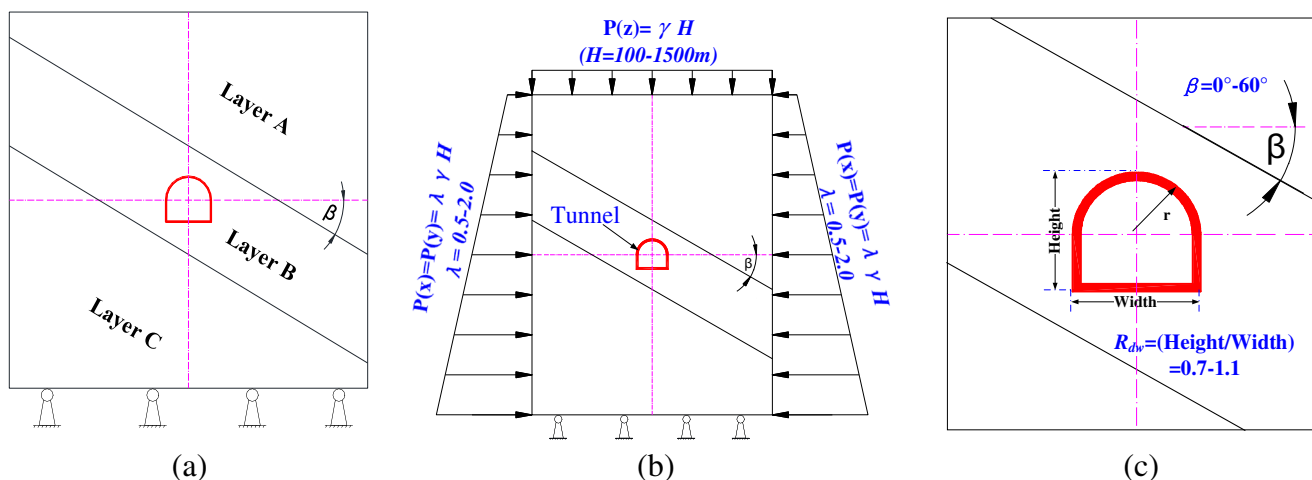| Test groups	Influence factors					
	Dip angle (β)/°	Lateral pressure coefficient (λ)	Burial depth (H)/m	Lithology	Height-width ratio (R_{dw})	Null
G1	0°	0.5	100	I	0.7	0
G2	0°	0.67	800	IV	1.1	1
G3	0°	1	1500	II	1	2
G4	0°	1.5	450	V	0.9	3
G5	0°	2	1150	III	0.8	4
G6	15°	0.5	1500	IV	0.9	4
G7	15°	0.67	450	II	0.8	0
G8	15°	1	1150	V	0.7	1
G9	15°	1.5	100	III	1.1	2
G10	15°	2	800	I	1	3
G11	30°	0.5	1150	II	1.1	3
G12	30°	0.67	100	V	1	4
G13	30°	1	800	III	0.9	0
G14	30°	1.5	1500	I	0.8	1
G15	30°	2	450	IV	0.7	2
G16	45°	0.5	800	V	0.8	2
G17	45°	0.67	1500	III	0.7	3
G18	45°	1	450	I	1.1	4
G19	45°	1.5	1150	IV	1	0
G20	45°	2	100	II	0.9	1
G21	60°	0.5	450	III	1	1
G22	60°	0.67	1150	I	0.9	2
G23	60°	1	100	IV	0.8	3
G24	60°	1.5	800	II	0.7	4
G25	60°	2	1500	V	1.1	0

Fig. 4 The boundary condition diagram of each test model. (**a**) Layers distribution, (**b**) boundary conditions, and (**c**) enlarged partial view

points in each experiment group was obtained, as shown in Figs. 5, 6, 7, 8, and 9a~e, respectively. The displacement of the nodes is absolute displacement.

Reference group

As shown in Fig. 5, in the horizontal rock layer, the maximum displacement is mostly located in the arch crown or the midpoint of roadway floor. In the arch part of the roadway, the value T_m of each monitoring point is mostly equal to the value T_u. The minimum displacement is mostly at the monitoring points NO. 1 and point NO. 21, and the arch camber points of the roadway have the same deformation magnitude. Moreover, with the increase of λ, the displacement difference between the arch crown and the arch camber points of the surrounding rock surface will gradually decrease.

On the straight wall and the floor of the roadway, the value T_m is slightly greater than the value T_u. The displacement accumulated to the maximum displacement and then fell back to some extent until deformation stability in some monitoring points. The magnitude of the fall back is related to the deformation of surrounding rock. The minimum displacement is mostly at the monitoring points NO. 26 and NO. 36. The positions of two feet of the roadway hold the same displacement. Therefore, the deformation of the surrounding rock is distributed symmetrically.

Asymmetric deformation under dip angle 15°

Under the 15° formation dip angle, the distribution locations of the maximum and the minimum displacement of the monitoring points have all migrated, shown in Fig. 6. The deformation of the arch part of the roadway is no longer

symmetrically distributed. The displacement magnitude on the arch crown right side (monitoring points NO. 8~NO. 10) are less than that on the left side (monitoring points NO. 12~NO. 14). The deformation of the arch crown is deflected downward to the lower part wall of the roadway. In the non-arch part of the roadway, the maximum value of T_m is still mostly distributed at the midpoint of the roadway floor. However, compared with the horizontal stratum, the value T_m on the left side of the floor is slightly larger than that of the corresponding monitoring point on the right side.

On the floor and two side straight walls of the roadway, the T_u curve and the T_m curve of the monitoring points do not completely coincide, shown in Fig. 6. The displacement still appears the phenomenon of deformation fall back. The deformation process is like that of the horizontal strata. The minimum displacement of the monitoring points is mostly at the monitoring point NO. 26 or NO. 36, the position of the roadway feet, and moving toward the straight walls of the roadway. Meanwhile, the displacement of the two feet becomes not equal, and the size relationship varies with the setting of the model influencing factors.

Asymmetric deformation under dip angle 30°

Under the 30° formation dip angle, the T_u and T_m curves fluctuate with the change of the monitoring points, shown in Fig. 7. The value T_m of the arch crown monitoring point is no longer the maximal value. The deformation changing proportion of the monitoring points close to the arch crown has gradually decreased.

On the floor of the roadway, the maximum displacement is still mainly distributed at the midpoint of the floor (monitoring point NO. 31). The displacement on the left half section near the floor midpoint is greater than that on the right half section.
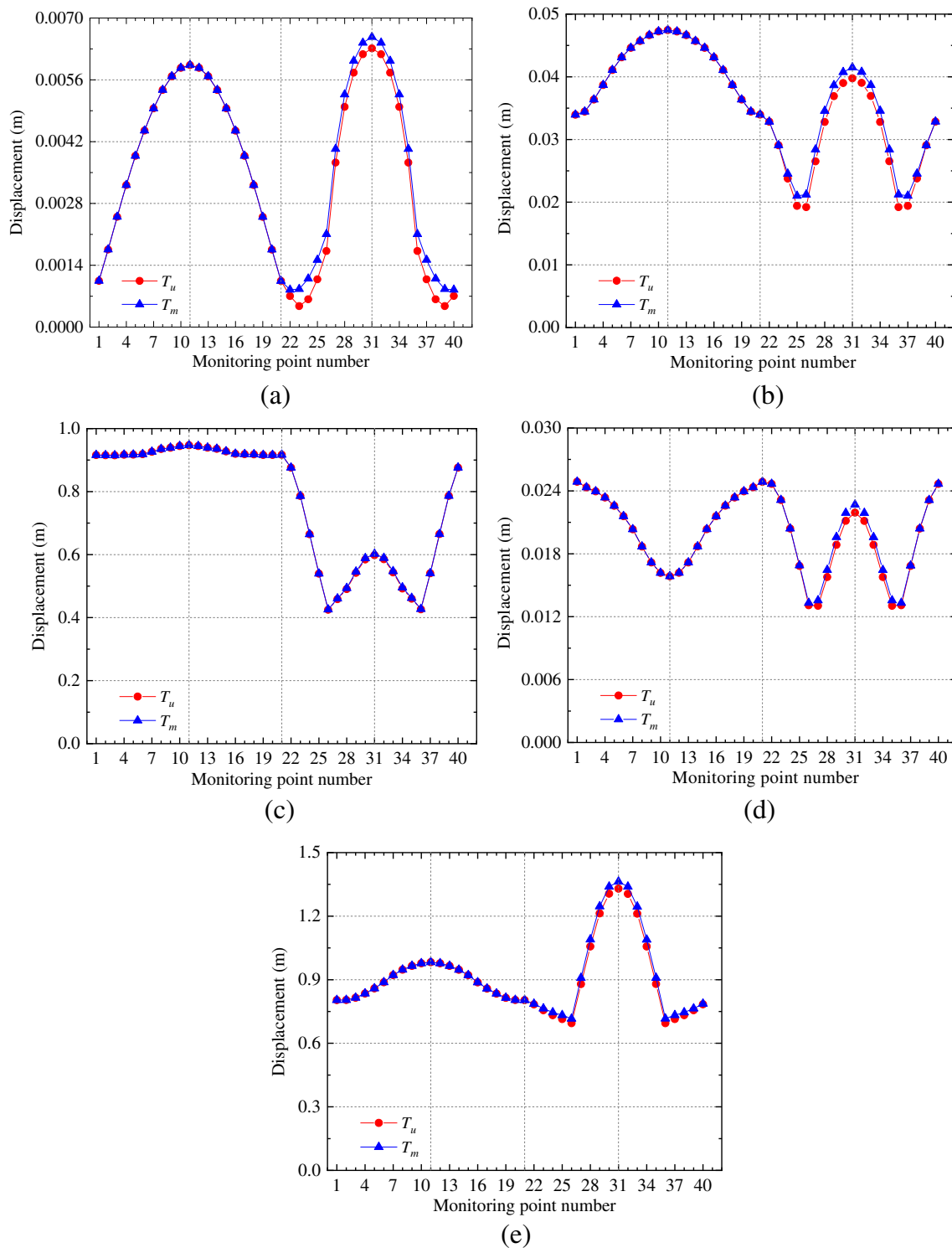
Fig. 5 Displacement curves under the horizontal strata. (a) G1, (b) G2, (c) G3, (d) G4, and (e) G5

The floor appears distinctly unequal deformation between the left and right half sections, that is, the asymmetric floor heave, and the maximum deformation is on the left of the floor mid-point. At the two feet (monitoring points NO. 26 and NO. 36), the deformations were also shown asymmetric deformation.

When λ is less than 1, the displacement of the upper part foot is slightly larger than that of the lower part foot. With increasing of λ, the displacement of the upper part foot is increasingly reduced till smaller than that of the lower part foot, and the deformation of the two feet is simultaneously affected by R_{dw}.
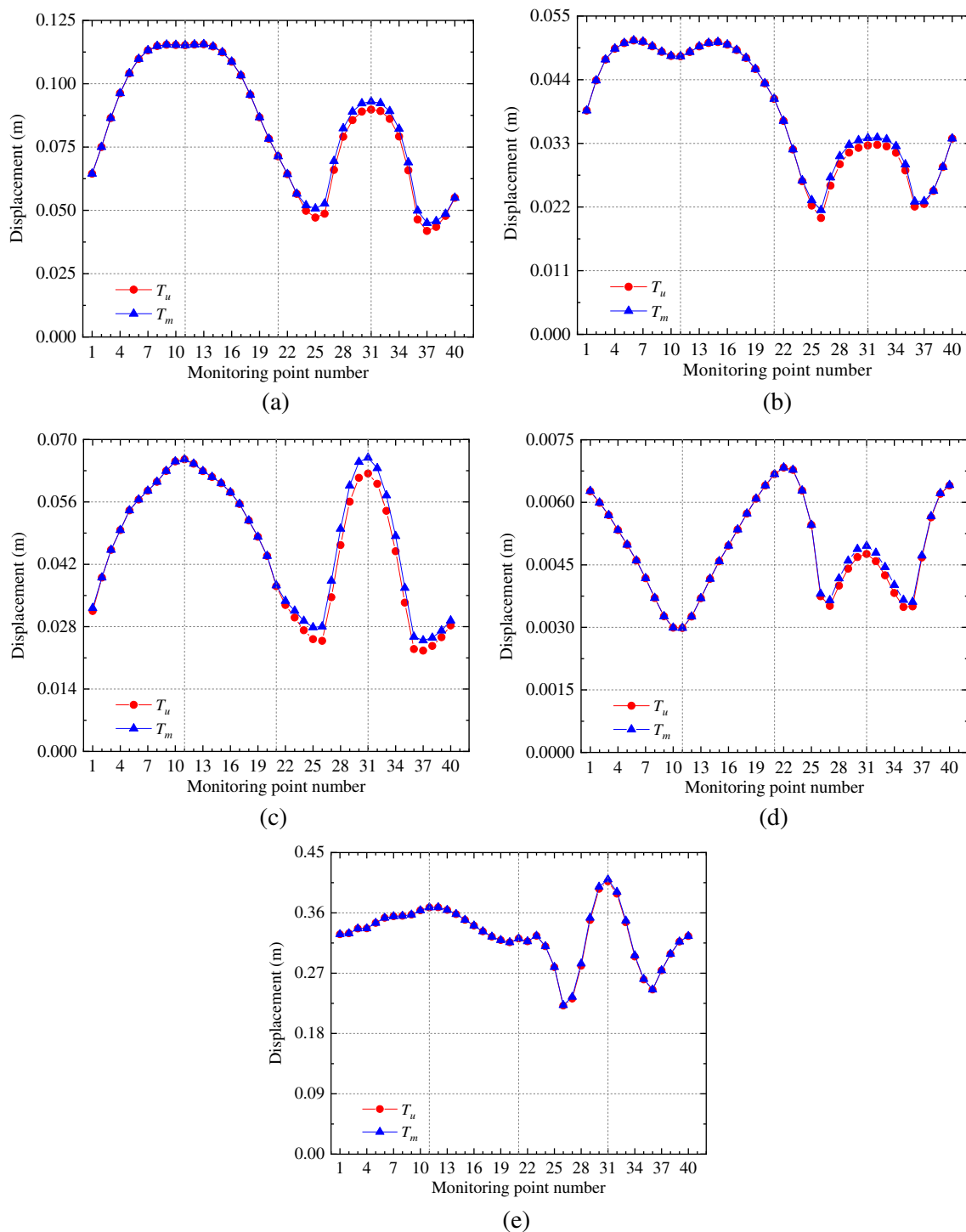
Fig. 6 Displacement curves under the strata with 15° dip angle. (**a**) G6, (**b**) G7, (**c**) G8, (**d**) G9, and (**e**) G10

Asymmetric deformation under dip angle 45°

Under the 45° formation dip angle, the T_m value and the T_u value of the arch crown are mostly smaller than that of the monitoring points on both sides of the arch crown, shown in Fig. 8. Notably, the deformations of the arch crown are all smaller than the deformations of the roadway floor midpoint,

and the difference between the two is basically keeping constant.

On the arch part of the roadway, with the increase of λ, the displacement difference between the lower arch shoulder and upper arch shoulder of the roadway decreased at first and then increased. When λ is less than 1, the minimum displacement is mainly located in the lower part arch camber point
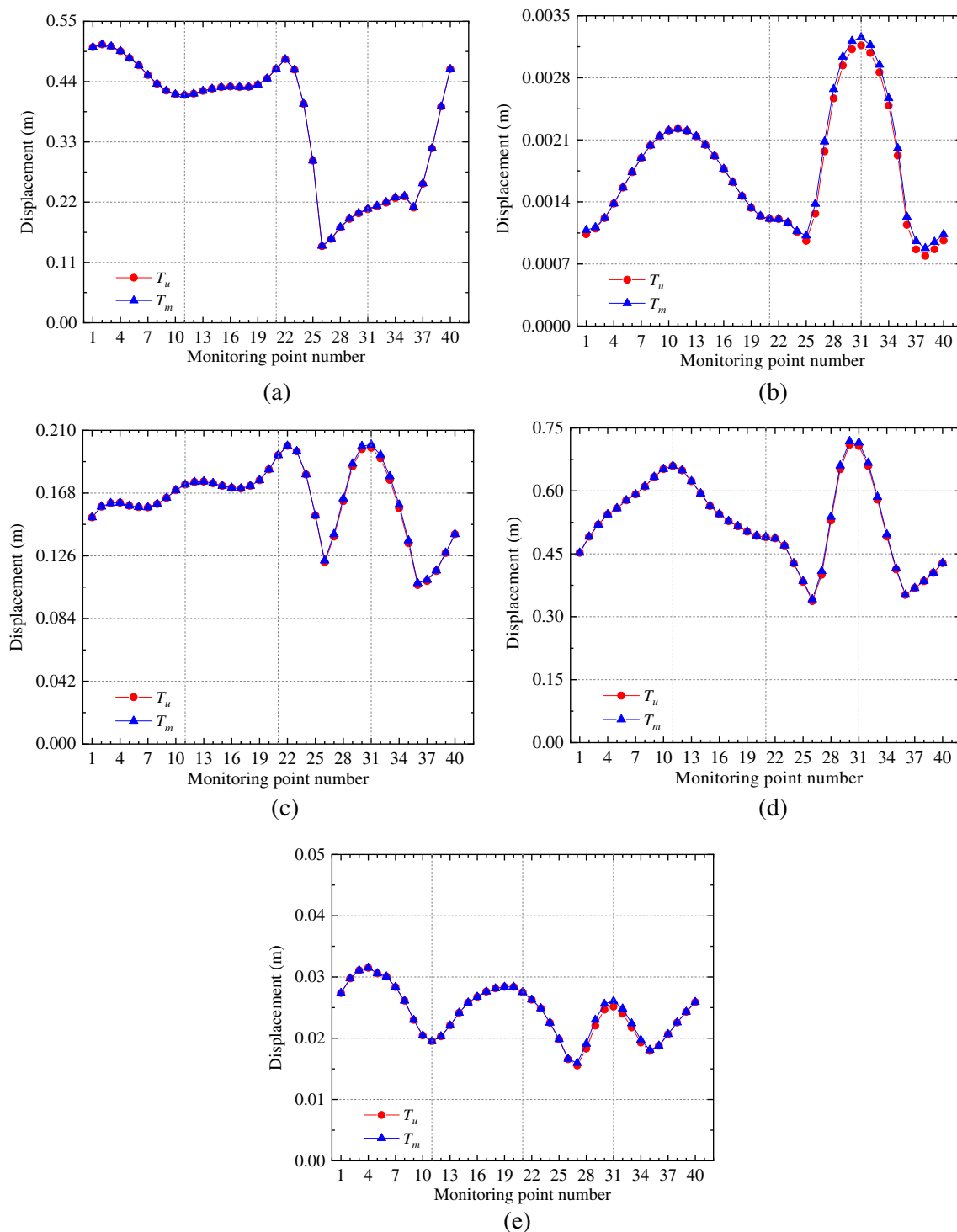
Fig. 7 Displacement curves under the strata with 30° dip angle. (a) G11, (b) G12, (c) G13, (d) G14, and (e) G15

(monitoring point NO. 1). When λ is greater than 1, the deformation of the lower arch shoulder has increasingly become larger than that of the upper arch shoulder of the roadway. In addition, with the increase of λ, the deformation difference between the arch crown and the two sides arch camber point will also decrease at first and then increase. The larger or smaller the λ, the deformation difference between the arch

crown and the arch camber points will be bigger. The deformation of the two sides arch camber point gradually increases.

On the floor of the roadway, the maximum of the values T_u is mainly distributed at the monitoring point NO. 30 or NO. 31. The roadway floor has a more noteworthy asymmetric floor heave deformation than that in the 15° and the 30° dipping formation. Similar to the case of 30° dipping
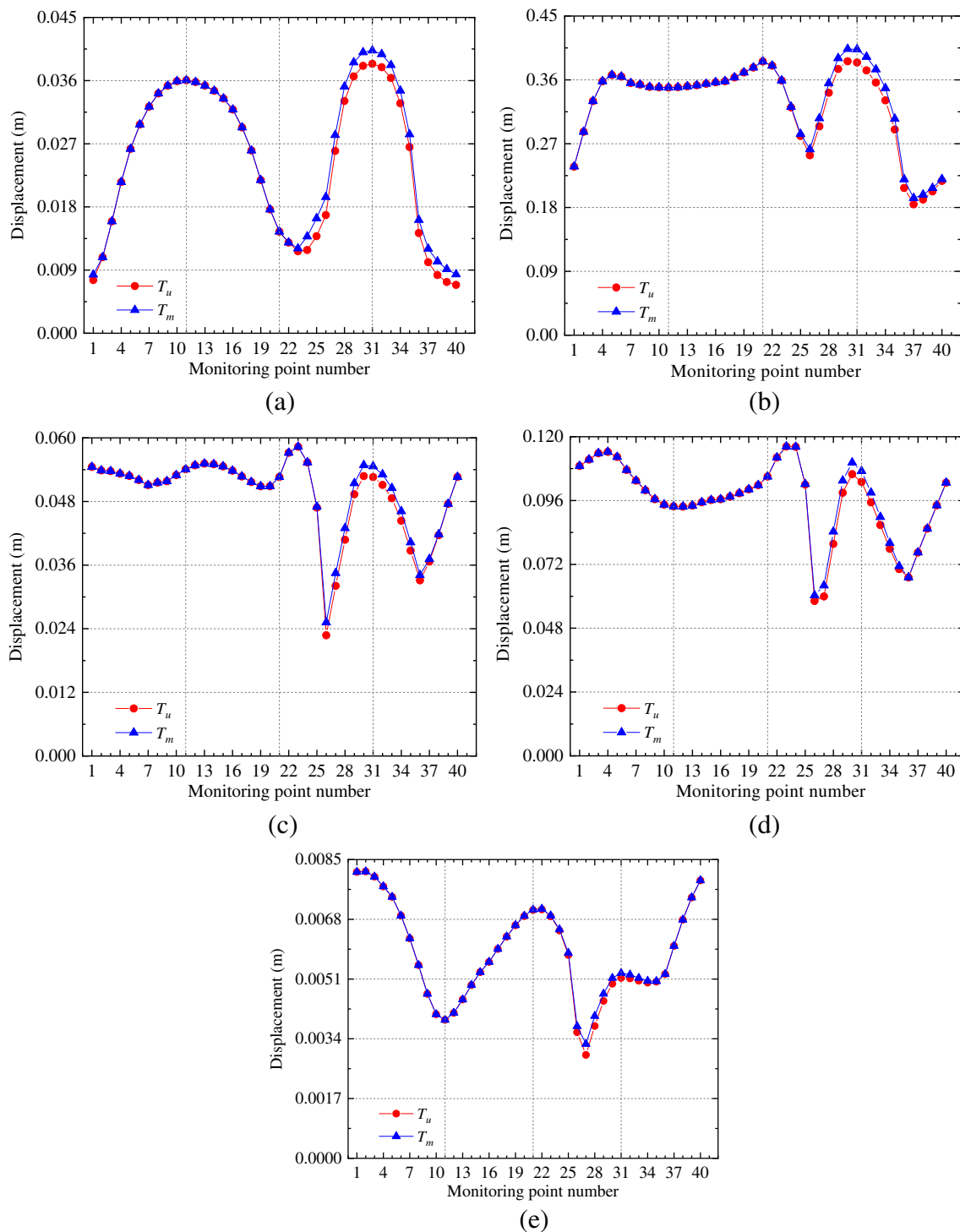
Fig. 8 Displacement curves under the 45° strata dip angle. (**a**) G16, (**b**) G17, (**c**) G18, (**d**) G19, and (**e**) G20

formation, the deformation on the left and right half section of the floor is significantly affected by the change of λ. The deformation of the two feet still emerges the asymmetric deformation phenomenon. When λ is less than 1, the deformation of the upper part foot (monitoring points NO. 26) is greater than the lower part foot (monitoring points NO. 36). With the increase of λ, the deformation difference of the two feet is gradually reduced until the difference is negative. That is the lower part foot greater than the upper part foot, in which λ is greater than 1. The T_u and T_m curves are still not coincidental in the monitoring points on the two straight walls and the floor of the roadway, accompanied by a small displacement fall back.
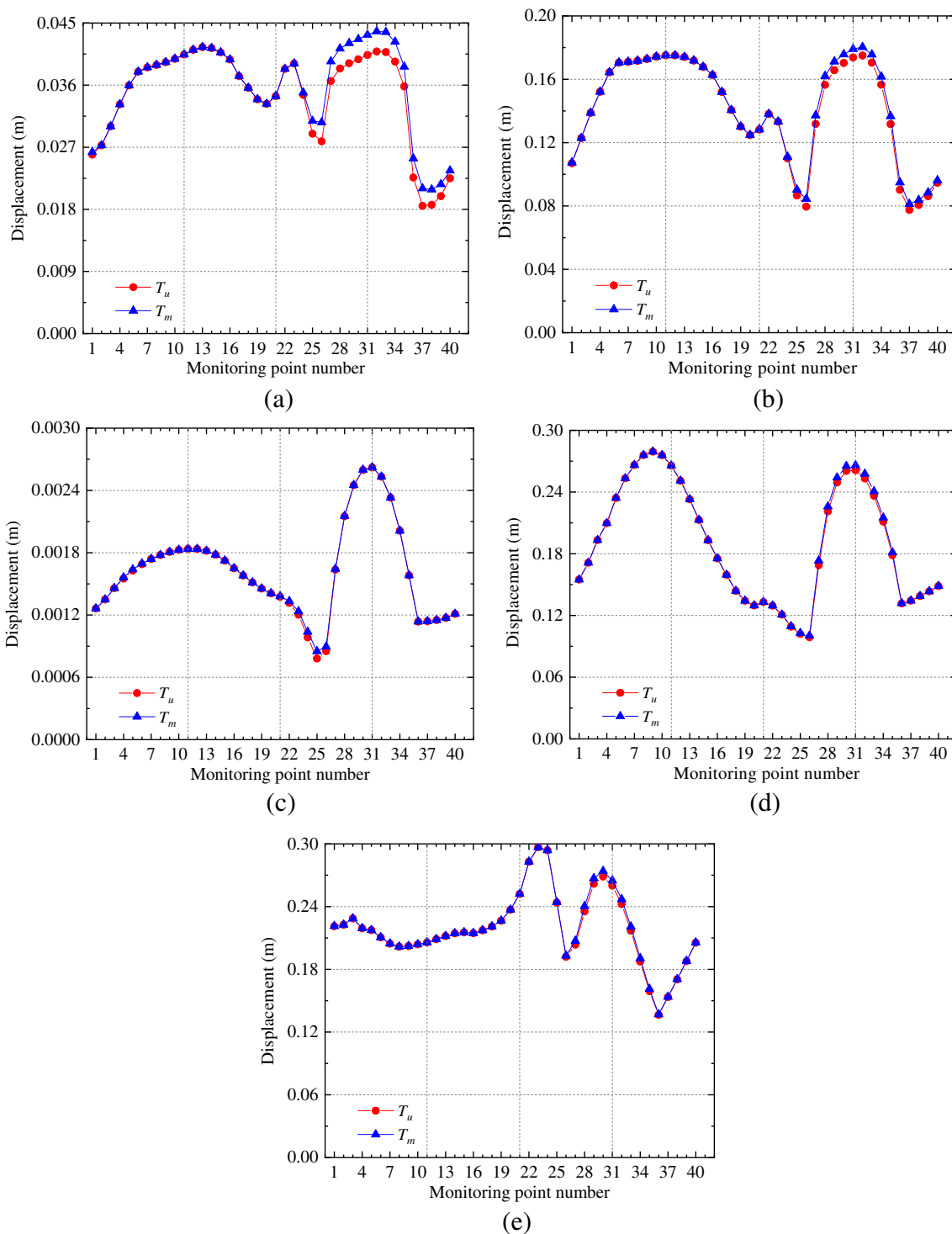
Fig. 9 Displacement curves under the strata with 60° dip angle. (**a**) G21, (**b**) G22, (**c**) G23, (**d**) G24, and (**e**) G25

Asymmetric deformation under dip angle 60°

Under the 60° formation dip angle, as shown in Fig. 9, the displacement fluctuation is much more complicated than that shown in Figs. 5, 6, 7, and 8. Under the higher R_{dw} (0.9 ~1.1), on the straight wall, the values T_m and T_u

of the monitoring points NO. 22 or NO. 23 became the extreme point of the neighboring monitoring points. Despite the different test conditions, the difference proportion of the maximum displacement between the arch part and the floor of the roadway is still small.

On the arch part of the roadway, the value T_m of the lower part arch camber point (monitoring point NO. 1) is smaller than that of the upper part arch camber point (monitoring point NO. 21). With the increase of λ, the difference of displacement deformation between the two arch camber points gradually decreases. The size relationship of the T_m value on both sides of the arch crown is also affected by λ. When λ is less than 1, the deformation of the lower arch shoulder is smaller than that of the upper arch shoulder. With the increase of λ, the deformation of the lower arch shoulder is increasingly close to till being larger than of the upper arch shoulder.

The displacement of few monitoring points on the roadway floor presents the phenomenon of displacement fall back shown in Fig. 9a~e. The minimum displacement is distributed at the upper part foot or lower part foot of the roadway. When λ is less than 1, the minimum displacement of the monitoring point is located in the lower part foot, while when λ is greater than 1, the minimum displacement is located in the upper part foot. But, it is broadly apparent that the location of the minimum displacement is combining affected by λ and R_{dw}. Comparing to λ, the R_{dw} has the opposite effect on the size relationship of the deformation between the two feet.

Discussions

In the deep inclined formation, the deformation of the surrounding rock of the roadway presents an asymmetry in spatial distribution. The λ and R_{dw} are the main factors affecting the asymmetric characteristics of surface deformation of the surrounding rock. For the straight wall semi-circular arch roadway, λ and R_{dw} affect the distribution position of the maximum and the minimum deformation of the monitoring points. They also determine the size relationship of displacement of the two feet.

The asymmetry characteristic will be attenuated when the formation dip angle exceeds 45°. Bounded by 45° inclined strata, under a smaller formation dip angle and a lower R_{dw}, when the λ is less than 1, the maximum deformations are the same as that of the horizontal strata. They are still at the position of the roadway arch crown. Meanwhile, the deformation of the upper part foot is greater than the lower part foot. As the λ increases, the position of the maximum deformation transfers to the midpoint of the floor. The displacement of the upper part foot is smaller than that of the lower part foot. With R_{dw} increasing, when λ is less than 1, the position of the maximum deformation (compared to R_{dw} is smaller) is gradually turned from the arch crown to the vicinity of the upper part arch camber point (monitoring point NO. 21), while under the higher R_{dw}, with the increase of λ, the position of the deformation maximum will gradually transfer back to the arch crown of the roadway. Above works can be used to forecast the surrounding rock deformation of the roadway in deep inclined strata. As we only set one level (60°) of the dip angle exceeds 45°, the combined effect of the λ the R_{dw} and the formation dip angle exceeding 45° on the asymmetric characteristics should be further investigated in the future. The following case study can be regarded as an attempt to predict and control the deformation of surrounding rock in steeply inclined strata.

Case study

Engineering background

A coal mine is in the south wing of the Xieqiao syncline in Huainan, North China. The mining area has a monocline structure, south dip, with a formation dip angle of 55 to 70°, an average of 60°, and a trend of 255 to 290°. The coal seam mining layer is 11-2 coal, the average thickness is 3.3m, and the 11-3 coal seam is 0.2m thick; the 11-1 coal seam is 0.3m thick. The 11-2 coal direct roof is carbonaceous mudstone with a thickness of 4.3m. The interlayer of 11-1 coal and 11-2 coal is grey-black mudstone with a thickness of 1.9m. During the roadway excavation process, many local pinch-out phenomena and many plant fossil fragments are found in the direct roof and the direct floor. The lithology is relatively close. Therefore, when selecting the stratum above and below the roadway in the numerical modelling process, 11-3 coal, 11-2 coal, 11-1 coal, and the direct roof and direct floor of the 11-2 coal are interbedded layers of coal mudstone with a total thickness of 10.0m. The comprehensive geological columnar section is shown in Fig. 10. The physical parameters of the rock layers are shown in Table 5.

Modelling

The model diagram of the coal exploration roadway is established, shown in Fig. 11. The model is set to a long rectangle with the model size of 52.8m×30m×111.46m (length × width × height). The model has 78,320 nodes and 73,350 elements. The section size of the roadway is 4.4m×3.5m (width × height), in which the R_{dw} is about 0.796. The designed buried depth is about −800m, so set the load on the model top to be −17.85MPa. According to the existing geological survey data of the mine, the λ of the strata was 1.5.

The roadway adopts the support scheme with 36U steel centering. The rock bolt is Φ20×2000mm, and row and line space is 800×800mm. The anchor cable is Φ17.8×6300mm, and row and line space is 1600×1600mm. The thickness of the shotcrete is 100mm, and space of the U-shaped steel shed is 1200mm. Modelling of the existing support scheme is shown in Fig. 12. The shotcrete and the steel centering cushion are simulated with the shell structural units and approximately

Fig. 10 Comprehensive geological columnar section

No.	Column	Lithology	Thickness /m	Geological description
1		Siltstone 1	17.63	Light gray, gray, dense and hard, fractures slight development
2		Mudstone	19.60	Brown, thick layered sandy mudstone, dense, brittle, containing plant fossil fragments
		Siltstone quartz sandstone	8.50	Light gray, grayish white, thick layered quartz sandstone, dense and hard, partial light gray siltstone
3		Coal mudstone interbed	10.0	Coal 11-2,11-3,11-1, gangue mainly sandy mudstone, large amounts of plant fossil fragments, partial pinching out
4		Sand mud interbed	23.40	Gray ,gray-black, thick layered sandy mudstone, mudstone interbed, dense, rich in plant fossil fragments
5		Sandy mudstone	6.70	Gray, rust-yellow quartz sandstone, medium-grain structure, crack development, quartz mineral, containing black mineral
6		Quartz sandstone	8.80	Gray-white, medium and coarse grain structure, fissure development, mainly quartz mineral composition
7 8		Siltstone 2	6.83	Light gray, dense and hard, fractures moderate development

calculated according to the C20 concrete strength parameters. The material parameters of structural units are shown in Table 6.

Deformation of the roadway

The roadway carries the conditions 60° formation dip angle, the $R_{dw}\approx0.796$, and the $\lambda=1.5$. Combined with the previous content, it belongs to higher λ, medium R_{dw}, and steeply inclined roadway. We can forecast the deformation of the roadway: the maximum of the surrounding rock should still be nearby the arch crown close to lower part wall or the midpoint of the floor close to upper part wall. The two feet hold unequal deformation magnitude, of which the upper part foot should be smaller than that of the lower part foot. For comparison and further investigating the influence of the support measures application on the stability of the roadway, we add the deformation of the unsupported roadway, which was set to be the

numerical simulation reference group; the displacement contours are shown in Fig. 13a.

The unsupported surrounding rock presented noticeable asymmetric deformation, shown in Fig. 13a. The displacement of the upper part arch camber point is larger than the lower part arch camber point. The displacement of each monitoring point on the upper part straight wall is greater than that of the corresponding monitoring point on the lower part straight wall, except for the upper part foot. The variation law of the surrounding rock surface deformation is basically consistent with the forecasting trend. As shown in Fig. 13b, under the existing support scheme, the surrounding rock deformation near the arch part of the roadway is controlled, and the displacement is comparatively small. From the arch shoulders to the arch camber points, the displacement gradually increases. Notably, the deformation on the arch part is symmetrically distributed now, and the deformation of each monitoring point is smaller than that of the straight walls and the floor of the roadway.

Table 5 Rock layer physical parameters of the coal exploration roadway

| NO.	Layer lithology	Layer depth H/(m)	Density ρ/(kg/m³)	Elastic modulus E/(GPa)	Poisson's ratio/ν	Tensile strength σ_t/(MPa)	Cohesion c/(MPa)	Friction φ/(°)
1	Siltstone	17.63	2600	10.0	0.25	3.80	3.42	37.0
2	Siltstone and quartz sandstone	19.6	2710	11	0.28	3.75	2.82	31.2
3	Mudstone	8.5	2433	4	0.30	1.73	0.746	29.0
4	Coal mudstone interbed	10.0	1800	2.5	0.31	0.80	0.80	20.5
5	Sand mud interbed	23.4	2635	6	0.3	1.21	0.907	28.6
6	Sandy mudstone	6.7	2605	6	0.3	1.45	0.746	30.8
7	Quartz sandstone	8.8	2580	12	0.23	5.67	4.792	28.6
8	Siltstone	6.83	2620	10	0.25	3.8	2.52	38.5
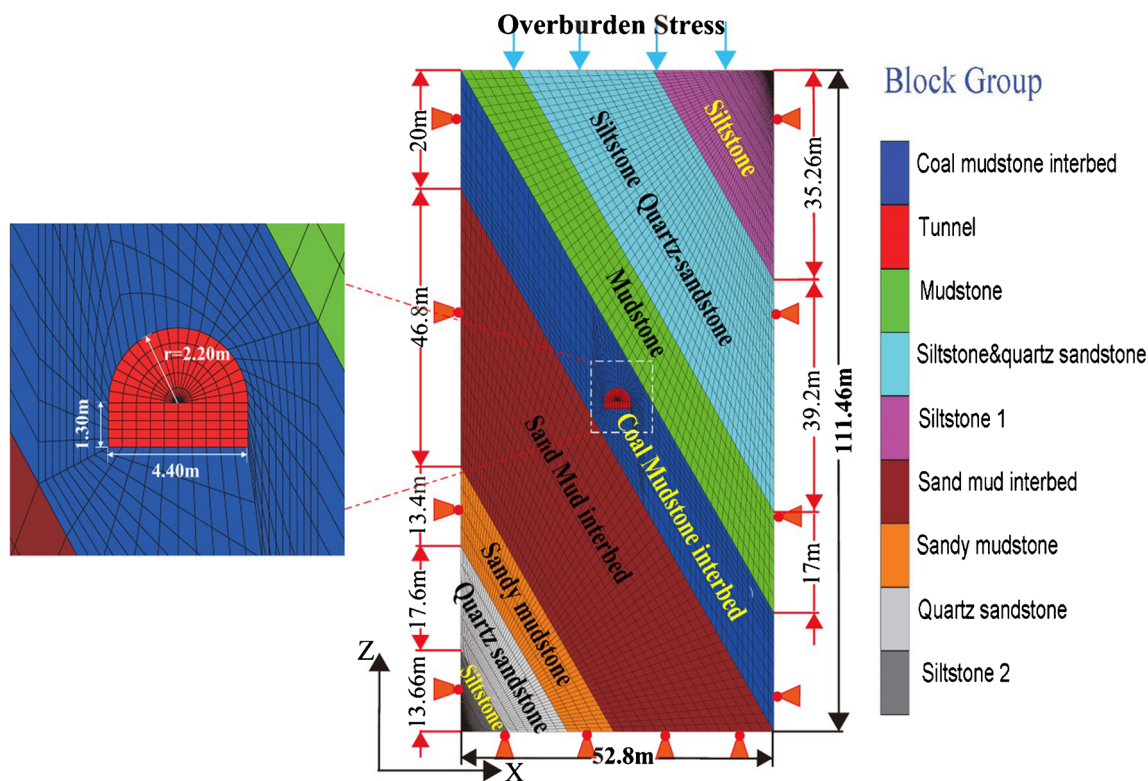
Fig. 11 Model diagram of the coal exploration roadway

As shown in Fig. 14, on the arch part of the roadway, when the surrounding rock is unsupported, the maximum displacement locates at the monitoring point NO. 10, while under the existing support scheme, the deformation of the arch part of the roadway is controlled, and the displacement is comparatively small. The deformation variation range of the supported surrounding rock at the arched part is about 25% of the maximum deformation. From the part arch camber points to the arch shoulders, the displacement of each monitoring point gradually decreases. The deformation of the supported surrounding rock in the arch part is symmetrically distributed now. On the floor, the maximum displacement of both the two cases locates at the monitoring point NO. 30. The deformation variation range of the floor is relatively large, nearly 60% of the maximum deformation. The floor deformation nearby the upper part is greater than that to the lower part.

The deformation of the upper part foot is still slightly larger than that of the lower part foot.

Although the arch settlement is better controlled, because of the large lateral deformation, the steel arch is bent from the two sides to the inside of the roadway. The arch is bent upward at the arch crown to resist the settlement of the roadway, even reverse deformation sometimes (Wang et al. 2015). It can be concluded that the existing support scheme satisfies the support requirements to a certain extent, and the deformations of the arch and the straight walls are controlled. The support scheme has suppressed the asymmetry of the surrounding rock deformation of the roadway surface. According to the on-site production survey, the roadway serviced less than 6 months and had to largely repair. The deformation control of the surrounding rock on the floor should be further added and reinforced.

Table 6 Structural element material parameter table

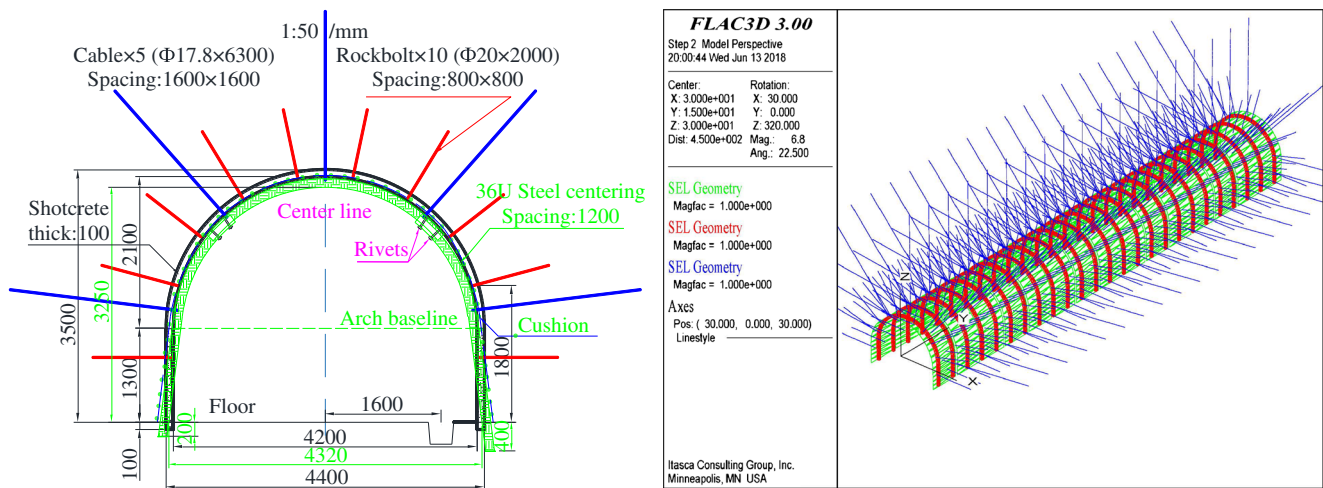| Support elements	Structure elements	Elasticity modulus E/(GPa)	Poisson ratio ν	Density ρ/(kg/m³)	Yield strength σ_s/(MPa)	Ultimate strength σ_b/(MPa)
Rock bolts	Cables	200	0.3	7850	500	700
Cables	Cables	200	0.3	7850	1700	1800
Shotcrete	Shell	25.5	0.2	2500	20	30
Steel arch lefting	Liner	190	0.3	7850	400	640

Fig. 12 Existing roadway support scheme and model diagram

Improved support scheme

In the deep roadway, the support scheme of closed steel arch with inverted arch is often adopted to control the floor heave in the coalmine roadway (Zhao et al. 2015). When carrying out the inverted arch support, the increase of the excavation section of the roadway is inevitable, and the depth selection of the inverted arch is the key to control the deformation of the floor heave. To achieve closed type support measures, we temporarily set the horizontal steel arches on the roadway floor instead of the inverted arch. Then, the supporting simulation analysis is carried out as shown in Fig. 15. For the structural unit parameters, shown in Table 6, the deformation of each monitoring point on the roadway surface is shown in Fig. 16

As the T_m and T_u curves shown, on the arch part and the two straight walls, the maximum deformation is located at the monitoring point NO. 20, and the displacement amount is about 0.0551m. Meanwhile, the deformations of the two arch camber points are about 0.0519m and 0.0474m, respectively, and the deformation difference is about 4.5mm. The deformations of the two feet are 0.0223m and 0.0233m, respectively. The difference is about 1mm. The deformation of the two sides is almost equal. After adding the horizontal steel arches on the floor, the deformation of the surrounding rock surface of the roadway is close to symmetrically distributed.

However, the deformation in the deep of the surrounding rock is still asymmetrically distributed to some extent, even though the deformation size has reduced, shown in Fig. 16a. The maximum deformation located at the midpoint of the floor and the displacement is 0.1036m. Compared with the
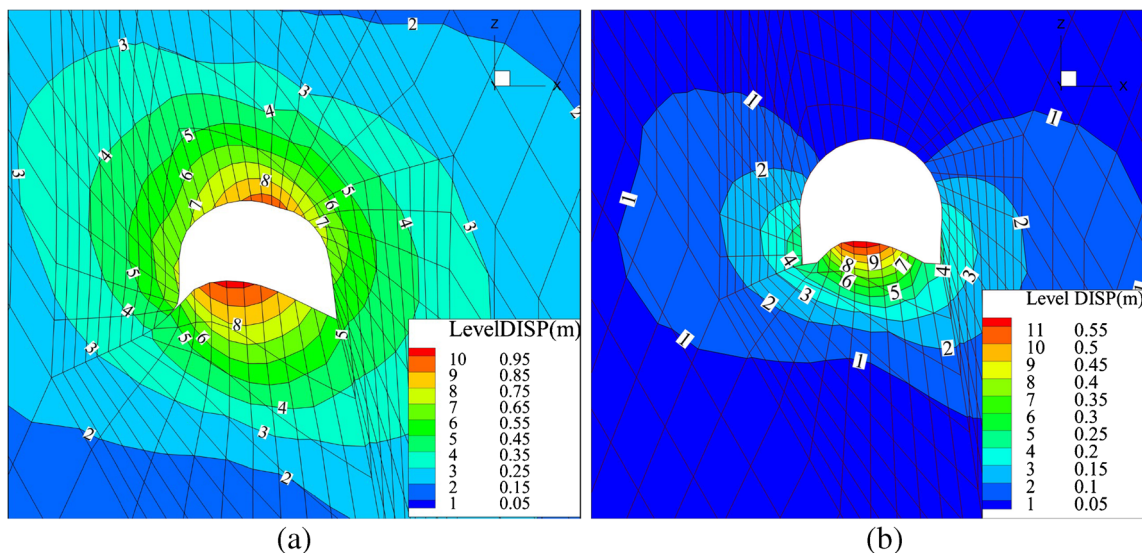

Fig. 13 Displacement contours of surrounding rock. (**a**) Unsupported roadway and (**b**) supported roadway

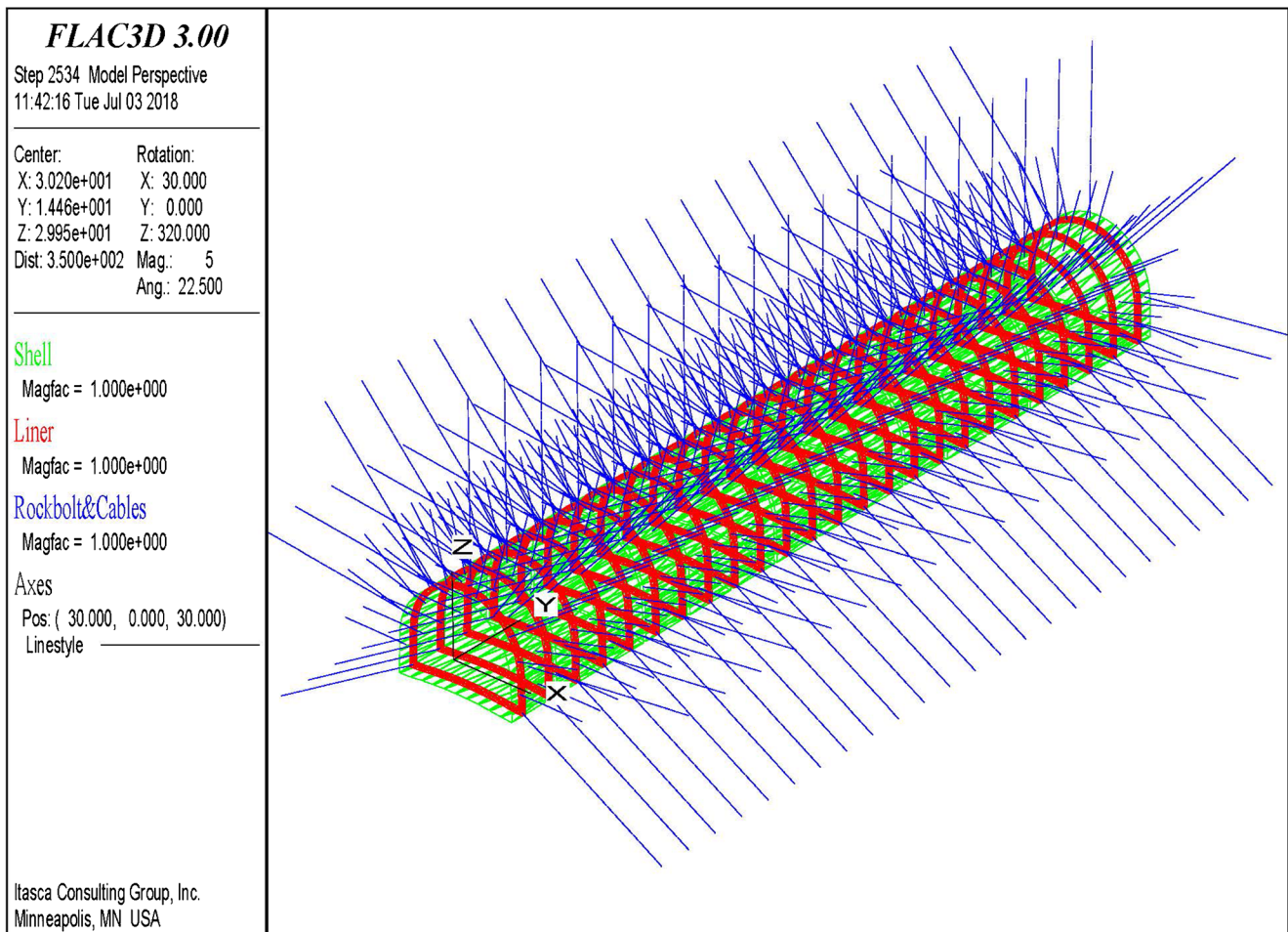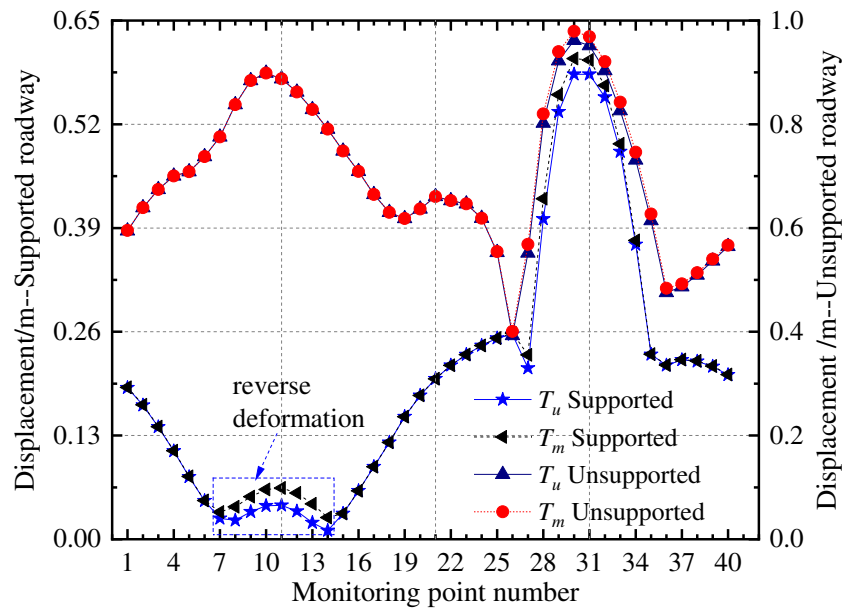**Fig. 14** Displacement curves of surrounding rock

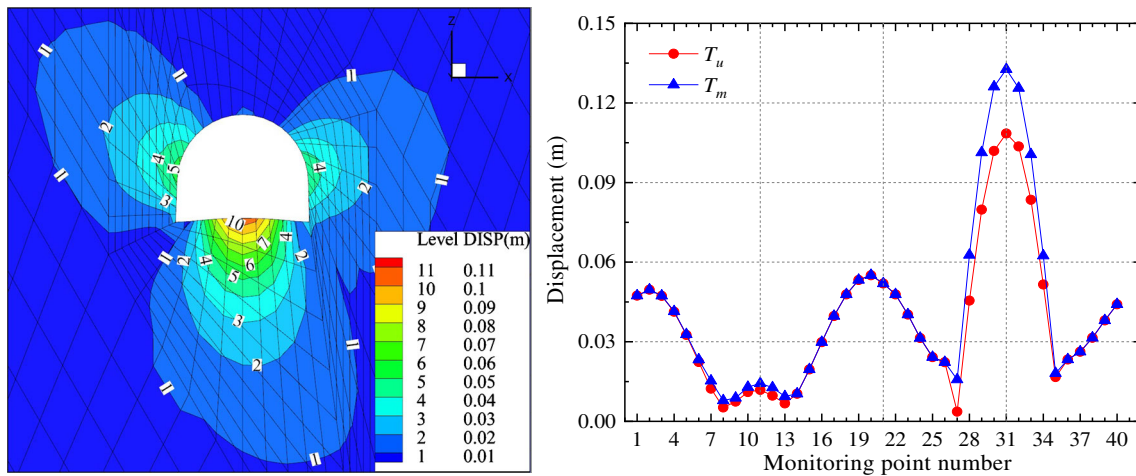**Fig. 15** Model diagram of horizontal bottom arch support form

Fig. 16 Displacement under horizontal bottom arch support (**a**) displacement contour of the surrounding rock **b**) displacement curves of the monitoring points

existing support scheme, a deformation of 0.5826m, the deformation reduction ratio is 82.22%. Therefore, the overall bearing capacity of the enclosure structure is improved to a great extent. To ensure the normal service of the roadway, we suggest that the depth of the inverted arch of this roadway should not be less than 103.6 mm.

Compared with the unclosed type arch support scheme, the deformation of the surrounding rock at each corresponding position reduced. The deformation control ratio is shown in Fig. 17. The primary support scheme better controlled the convergence of the arch camber points on the two straight walls, especially the settlement of the roadway arch crown. The deformation control ratios were 69.6%, 68.1%, and 95.2%, respectively. The asymmetry of the deformations of the two straight walls improved, and the convergence rate of the monitoring points reduced from the original difference of 10.0% to 5.47%. The asymmetry of the deformation on the two feet also changed. The ratio of the deformation difference varies from −21.12 to 15.18%. Thus, when the deformation difference of the surrounding rock of the two feet decreased, the size relationship also reversely changed. The deformation control ratio of the two feet was 34.7% and 54.2%, respectively.

With the improved support measures, the deformation of the surrounding rock further reduced, and the deformation is close to the symmetric distribution. Compared with the primary support scheme, the secondary deformation control ratio of the roadway floor is 81.38%. The total secondary deformation

Fig. 17 Deformation and control ratio under different support schemes
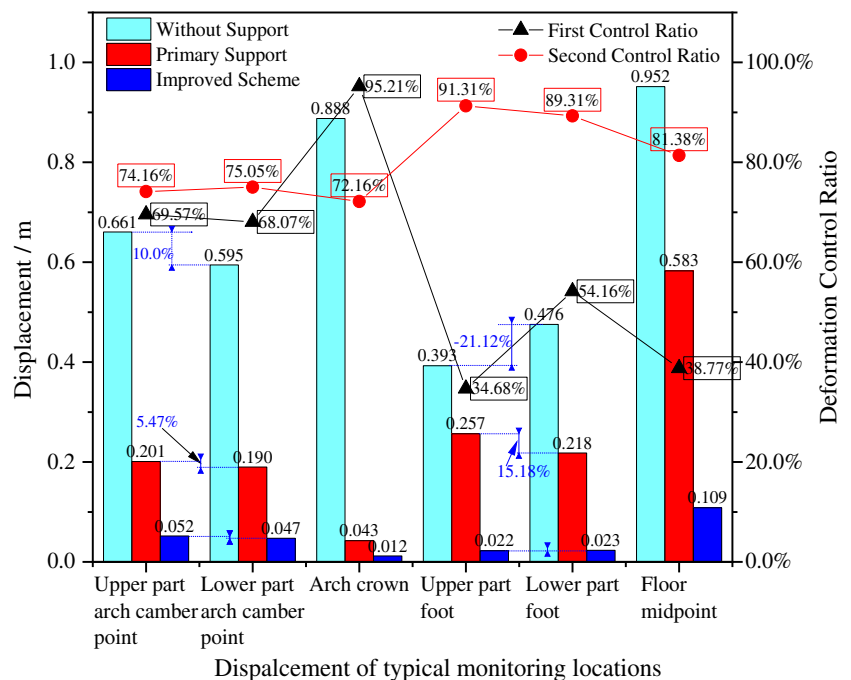
control ratio of the surrounding rock is more than 72.16%. The deformation of the surrounding rock reduced, which can meet the normal production requirements of the roadway.

Conclusions

A full-section nodes' displacement monitoring and recording method of the surrounding rock surface was proposed to investigate the asymmetry of surrounding rock deformation. Based on orthogonal experiments, we numerically simulated and analyzed the asymmetry of the deformation under different conditions. The combined effects of the burial depth and height-width ratio R_{dw} of the roadway, lithology, dip angle, and lateral pressure coefficient λ of the layers on the asymmetric deformation of roadway surrounding rock were concluded. The asymmetric deformation features and improved support scheme design of a site roadway were studied. Conclusions can be drawn:

(1) The deformation law and asymmetry feature of the surrounding rock were obtained with the full-section displacement monitoring and recording method. The phenomenon displacement falling back between T_u and T_m curves mostly appears at the stagnation point of the monitoring point deformation curve. The position of the stagnation point is mainly distributed at the side feet of the roadway, sometimes near the midpoint of the floor, where the most significant asymmetric deformation of the roadway will present.

(2) The increase of the formation dip angle within a certain range will aggravate the asymmetry of the deformation. The most significant asymmetric deformation occurs when the dip angle is 45°. When the formation dip angle exceeds 45°, the asymmetric deformation of the surrounding rock gradually weakens.

(3) λ and R_{dw} significantly affect the asymmetry of the deformation. The increase of λ will change the distribution position of the maximum deformation of the surrounding rock, especially the maximum deformation position of the arch part of the roadway. The R_{dw} mainly determines the deformation magnitude relation of the two straight walls.

(4) The application of the closed type support measures remarkably reduced the size and asymmetry of the surface deformation of the surrounding rock. With the improved support scheme, the surface deformation of the surrounding rock is close to symmetrically distributed. Compared to the primary support scheme, the secondary deformation control ratio is no less than 70%, which can provide a reference for the deformation control of the deep roadway.

Declarations

Conflict of interest The authors declared that they have no conflicts of interest to this work.

References

Cao P, Li HY, Zhong YF, Wang F (2017) Mechanism and control of floor heave of deep buried roadway with high lateral pressure coefficient. J Cent South Univ 48(2):457-464. doi:10.11817/j.issn.1672−7207.2017.02.025 (in Chinese)

Chen J, Yan R, Liu K (2018a) Asymmetric deformation mechanism of roadway at steeply inclined thick coal seam. J China Coal Soc 43(11):3007–3015. https://doi.org/10.13225/j.cnki.jccs.2018.8021 (in Chinese)

Chen S, Wu A, Wang Y, Chen X, Yan R, Ma H (2018b) Study on repair control technology of soft surrounding rock roadway and its application. Eng Fail Anal 92:443–455. https://doi.org/10.1016/j.engfailanal.2018.06.006

Chen YX (2017) Influence of lithological characters and location on tunnel asymmetric deformation. Safty in Coal Mines 48(1):179–182 (in Chinese)

Chen YX, Gao MZ, Li LP, Shi SS, Zhou ZQ, Zhang MG (2020) Contributory factors and distribution characteristics of asymmetric deformation in deep tunnel. Geotech Geol Eng. https://doi.org/10.1007/s10706-020-01555-4

Das AJ, Mandal PK, Bhattacharjee R, Tiwari S, Kushwaha A, Roy LB (2017a) Evaluation of stability of underground workings for exploitation of an inclined coal seam by the ubiquitous joint model. Int J Rock Mech Min Sci 93:101–114. https://doi.org/10.1016/j.ijrmms.2017.01.012

Das R, Singh PK, Kainthola A, Panthee S, Singh TN (2017b) Numerical analysis of surface subsidence in asymmetric parallel highway tunnels. J Rock Mech Geotech 9:170–179. https://doi.org/10.1016/j.jrmge.2016.11.009

Ding XL, Niu XQ, Pei QT, Huang SL, Zhang YT, Zhang CH (2019) Stability of large underground caverns excavated in layered rock masses with steep dip angles: a case study. Bull Eng Geol Environ 78:5101–5133. https://doi.org/10.1007/s10064-018-01440-8

Dong WL, Chen YK, Zhi YQ, Shu J, Zhang JJ, Wang TT (2014) Research on electronic measuring technology with development of total station coordinate traverse adjustment program. Adv Mater Res 1014:371–374

Dzierzega A, Scherrer R (2003) Measuring with electronic total stations. Survey Review 37:55–65

Hayati AN, Ahmadi MM, Hajjar M, Kashighandi A (2014) Unsupported advance length in tunnels constructed using New Austrian tunnelling method and ground surface settlement. Int J Numer Anal Methods Geomech 37:2170–2185

He MC, Gao YB, Yang J, Wang JW, Wang YJ, Zhu Z (2018) Engineering experimentation of gob-side entry retaining formed

by roof cutting and pressure release in a thick-seam fast-extracted mining face. Rock Soil Mech 39(1):254–264. https://doi.org/10.16285/j.rsm.2016.2329 (in Chinese)

He MC (2011) Physical modeling of an underground roadway excavation in geologically 45° inclined rock using infrared thermography. Eng Geol 121:165–176. https://doi.org/10.1016/j.enggeo.2010.12.001

He MC, Peng YY, Zhao SY, Shi HY, Wang N, Gong WL (2015) Fracture mechanism of inversed trapezoidal shaped tunnel excavated in 45 degrees inclined rock strata. Int J Min Sci Techno 25:531–535. https://doi.org/10.1016/j.ijmst.2015.05.003

Huang F, Zhu H, Xu Q, Cai Y, Zhuang X (2013) The effect of weak interlayer on the failure pattern of rock mass around tunnel-scaled model tests and numerical analysis. Tunn Undergr Sp Tech 35:207–218. https://doi.org/10.1016/j.tust.2012.06.014

Huang WP, Yuan Q, Tan YL, Wang J, Liu GL, Qu GL, Li C (2018) An innovative support technology using a concrete-filled steel tubular structure for a 1000-m-deep roadway in a high in situ stress field. Tunn Undergr Sp Tech 73:26–36

Itasca Consulting Group I (2012) Fast Lagrangian analysis of continua in 3 dimensions user's guide. Itasca Consulting Group, Inc., Minneapolis ,Minnesota,USA.

Jiao YY, Song L, Wang XZ, Adoko AC (2013) Improvement of the U-shaped steel sets for supporting the roadways in loose thick coal seam. Int J Rock Mech Min Sci 60:19–25. https://doi.org/10.1016/j.ijrmms.2012.12.038

Lan H, Yao JG, Zhang HX, Xu NZ (2008) Development and application of constitutive model of jointed rock mass damage for mining based on FLAC3D. Chin J Rock Mech Eng 27(3):572–579 (in Chinese)

Lei M, Peng L, Shi C (2014) Calculation of the surrounding rock pressure on a shallow buried tunnel using linear and nonlinear failure criteria. Automat Constr 37:191–195

Li LP, Shang CS, Chu KW, Zhou ZQ, Song SG, Liu ZH, Chen YH. (2021). Large-scale geo-mechanical model tests for stability assessment of super-large cross-section tunnel. Tunn Undergr Sp Tech, 109, 103756. https://doi.org/10.1016/j.tust.2020.103756

Li SC, Wang Q, Wang HT, Jiang B, Wang DC, Zhang B, Li Y, Ruan GQ (2015) Model test study on surrounding rock deformation and failure mechanisms of deep roadways with thick top coal. Tunn Undergr Sp Tech 47:52–63. https://doi.org/10.1016/j.tust.2014.12.013

Li WT, Yang N, Yang B, Ma HY, Li TC, Wang Q, Wang G, Du YT, Zhao MX (2018) An improved numerical simulation approach for arch-bolt supported tunnels with large deformation. Tunn Undergr Sp Tech 77:1–12

Lin BQ, Liu T, Zou QL, Zhu CJ, Yan FZ, Zhen Z (2015) Crack propagation patterns and energy evolution rules of coal within slotting disturbed zone under various lateral pressure coefficients. Arab J Geosci 8:6643–6654

MacPherson WN, Silva-Lopez M, Barton JS, Moore AJ, Jones JDC, Zhao D, Zhang L, Bennion I, Metje N, Chapman DN, Rogers CDF (2006) Tunnel monitoring using multicore fibre displacement sensor. Meas Sci Technol 17(5):1180–1185. https://doi.org/10.1088/0957-0233/17/5/s41

Majcherczyk T, Niedbalski Z, Malkowski P, Bednarek L (2014) Analysis of yielding steel arch support with rock bolts in mine roadways stability aspect. Arch Min Sci 59:641–654. https://doi.org/10.2478/amsc-2014-0045

Mark C, Gale W, Oyler D, Chen J (2007) Case history of the response of a longwall entry subjected to concentrated horizontal stress. Int J Rock Mech Min Sci 44:210–221

Mu Z, Liu G, Yang J, Zhao Q, Javed A, Gong S, Cao J (2019) Theoretical and numerical investigations of floor dynamic rupture: a case study in Zhaolou Coal Mine, China. Safety Sci 114:1–11. https://doi.org/10.1016/j.ssci.2018.12.016

Ng CWW, Lee KM, Tang DKW (2004) Three-dimensional numerical investigations of New Austrian tunnelling method (NATM) twin tunnel interactions. Can Geotech J 41:523–539

Peng R, Meng XX, Zhao GM, Li YM, Zhu JM (2018) Experimental research on the structural instability mechanism and the effect of multi-echelon support of deep roadways in a kilometre-deep well. PLOS ONE 13(9):e0204059

Shen BT (2014) Coal mine roadway stability in soft rock: a case study. Rock Mech Rock Eng 47:2225–2238

Sun XM, Li G, Zhao CW, Liu YY, Miao CY (2019) Investigation of deep mine shaft stability in alternating hard and soft rock strata using three-dimensional numerical modeling. Processes 7(1):2. https://doi.org/10.3390/pr7010002

Sun XM, Chen F, He MC, Gong WL, Xu HC, Lu H (2017) Physical modeling of floor heave for the deep-buried roadway excavated in ten degree inclined strata using infrared thermal imaging technology. Tunn Undergr Sp Tech 63:228–243. https://doi.org/10.1016/j.tust.2016.12.018

Wang Q, Jiang B, Li Y, Shao X, Wang FQ, Li SC, Zhang SG, Ruan GQ (2015) Mechanical behaviors analysis on a square-steel-confined-concrete arch centering and its engineering application in a mining project. Eur J Environ Civ En 21:389–411. https://doi.org/10.1080/19648189.2015.1124809

Wang Q, Jiang B, Pan R, Li SC, He MC, Sun HB, Qin Q, Yu HC, Luan YC (2018) Failure mechanism of surrounding rock with high stress and confined concrete support system. Int J Rock Mech Min Sci 102:89–100. https://doi.org/10.1016/j.ijrmms.2018.01.020

Xia XY, Song Y, Fang DQ (2001) Influence of tectonic uplift on formation pressure and genesis of the abnormal pressure in KELA-2 Gas Field. Natur Gas Ind 21(1):30–34 (in Chinese)

Xie HP, Gao MZ, Zhang R, Peng GY, Wang WY, Li AQ (2019) Study on the mechanical properties and mechanical response of coal mining at 1000m or deeper. Rock Mech Rock Eng 52:1475–1490. https://doi.org/10.1007/s00603-018-1509-y

Yang C, Oyadiji SO (2016) Development of two-layer multiple transmitter fibre optic bundle displacement sensor and application in structural health monitoring. Sensor Actuat A-Phys 244:1–14

Yang SQ, Chen M, Jing HW, Chen KF, Meng B (2016) A case study on large deformation failure mechanism of deep soft rock roadway in Xin'An coal mine, China. Eng Geol 217:89–101

Yasitli, Erhan N (2013) Numerical modeling of surface settlements at the transition zone excavated by New Austrian tunneling method and umbrella arch method in weak rock. Arab J Geosci 6(7):2699–2708

Zeng LB, Zhou TW, Lv XX (2004) Influence of tectonic compression on the abnormal formation pressure in the Kuqa depression. Geological Review 50(5):471–475 (in Chinese)

Zhang YT (2014) Analysis of seepage field of highway tunnel excavation by finite difference method. Appl Mech Mater 638-640:798–803

Zhao Y, Liu N, Zheng X, Zhang N (2015) Mechanical model for controlling floor heave in deep roadways with U-shaped steel closed support. Int J Min Sci Technol 25:713–720. https://doi.org/10.1016/j.ijmst.2015.07.003